Sensors and Actuators B 186 (2013) 172–179

Contents lists available at SciVerse ScienceDirect

Sensors and Actuators B: Chemical

journal homepage: www.elsevier.com/locate/snb

# Rhombus-shaped $Co_3O_4$ nanorod arrays for high-performance gas sensor

Zhen Wen, Liping Zhu*, Weimin Mei, Liang Hu, Yaguang Li, Luwei Sun, Hui Cai, Zhizhen Ye

*State Key Laboratory of Silicon Materials, Department of Materials Science and Engineering, Cyrus Tang Center for Sensor Materials and Applications, Zhejiang University, Hangzhou, 310027, PR China*

ARTICLE INFO

*Article history:*
Received 27 February 2013
Received in revised form 26 April 2013
Accepted 27 May 2013
Available online 6 June 2013

*Keywords:*
Gas sensor
Facile synthesis
Rhombic $Co_3O_4$
Nanorod arrays
Ethanol sensing

ABSTRACT

Rhombic $Co_3O_4$ nanorod (NR) array-based gas sensor was successfully fabricated via a facile two-step synthesis approach, including the formation of rhombic Co(OH)F NR arrays as precursor followed by thermal conversion to porous $Co_3O_4$ without altering the original shape. Good ohmic contacts with the electrodes and intensive contact with the substrates avoided complicated fabrication process of gas sensors. The NR arrays annealed at 450 °C showed high-performance of ethanol detection. The response to 500 ppm ethanol gas reached ~71 and the optimal working temperature was as low as 160 °C. Meanwhile, the sensor exhibited good response/recovery kinetics (90 s and 60 s), outstanding selectivity over several interferential gases and good stability tested in 3 months. In addition, the sensor could detect ethanol at a low detection limit (<10 ppm), which exhibited good reproducibility. The high ethanol gas sensing performance of the $Co_3O_4$ NRs can be explained by a typical *p*-type behavior with the one-dimension structure, nano-porosity, large specific surface area, good crystallinity and the open space of nanorod arrays.



## 1. Introduction

Cobalt oxide ($Co_3O_4$) is considered to be one of the most representative *p*-type semiconductors and the most promising functional materials in many technological areas, such as heterogeneous catalysis, supercapacitors, lithium-ion batteries, and especially gas sensors [1–5]. In view of these profitable utilizations, a large number of efforts have been focused on the synthetic techniques of growing cobalt oxide nanostructures, including hydrothermal, electrospinning, chemical vapor deposition, sputtering and pulsed laser deposition, etc. [6–9]. Various nanostructures on synthesizing $Co_3O_4$ for gas detection were reported, such as meso- and macroporous $Co_3O_4$ nanorods for effective volatile organic compounds gas sensing [10], concave $Co_3O_4$ octahedral mesocrystal for formaldehyde and ethanol detection [11], and $Co_3O_4$ hollow nanospheres toward toluene and acetone vapors [12]. From the viewpoint of device structure, $Co_3O_4$ gas sensors have been usually synthesized in the form of thin films, in which the powders are screen printed on prefabricated electrodes ceramics tubes or insulative plates followed by annealing at the appropriate temperature. Nevertheless, only a small fraction of the species adsorbed near the grain boundaries in thin-film gas sensors is active in modifying the electrical transport properties, which are apt to lose the characteristic advantage of the larger length-to-diameter and surface-to-volume ratios than bulk materials and films for nanostructure building blocks resulting from agglomeration [13]. There is thus still an evident need for detailed investigations regarding the device structures.

On the other hand, the gas sensing performance of $Co_3O_4$ for ethanol detection which is closely related to the issues of public health and safety has been arousing great interest. Previously, Choi et al. have discussed that the gas responses of various $Co_3O_4$ nanostructures such as nanorods, nanosheets, and nanocubes to 100 ppm $C_2H_5OH$ at 300 °C were several times higher than those of the $Co_3O_4$ agglomerated nanopowders, respectively [14]. Cao et al. have synthesized $Co_3O_4$ with different morphologies which exhibited high performance at an operating temperature of 300 °C as an ethanol sensor [15]. Yoon et al. have fabricated the $Co_3O_4$ nanofibers which exhibited high responses (~51.2) to 100 ppm $C_2H_5OH$ at 301 °C [16]. All the above sensors have the optimal working temperatures at about 300 °C, which is too high for practical application. A large scale monodisperse porous flowerlike $Co_3O_4$ microspheres consisting of nanoplatelets showed enhanced ethanol sensitivity and selectivity at a relatively low temperature of 135 °C, however, with a low gas response at ~15 for 500 ppm ethanol [17]. Thus, fabricating gas sensors to ethanol based on $Co_3O_4$ which have high response at a low temperature is an uphill task. Nanoarray-based sensors are of particular interest because

* Corresponding author. Tel.: +86 571 87953139; fax: +86 571 87952625.
*E-mail address:* zlp1@zju.edu.cn (L. Zhu).

0925-4005/$ – see front matter © 2013 Elsevier B.V. All rights reserved.
http://dx.doi.org/10.1016/j.snb.2013.05.093

of not only low cost and great miniaturization potential, but also high reaction rate, which leads to a higher sensing performance. So far, huge amounts of works were focused on the *n*-type metal oxide semiconductor nanoarray-based gas sensors (e.g. ZnO, $SnO_2$, $TiO_2$) and most of the experimental and theoretical knowledge was focused on the *n*-type case [18–21]. Few works have dealt with *p*-type semiconducting metal oxide array-based gas sensors. Thus, exploring the gas sensing performance arising from the nanostructure arrays of *p*-type semiconductors is demanding.

Herein, we present the fabrication of the rhombus-shaped $Co_3O_4$ NR array-based gas sensor with high-performance for ethanol detection, whose fabrication process does not require expensive and complicated fabrication techniques. The characterization of the NR arrays was investigated by X-ray diffraction (XRD), Fourier transform infrared spectroscopy (FTIR), X-ray photoelectron spectroscopy (XPS), scanning electron microscopies (SEM), transmission electron microscopy (TEM) and high-resolution TEM (HRTEM). The NR arrays directly grow on the supporting substrates and intensive contact with the substrate supplies a simple method to prepare a nanoarray-based gas sensor without the conventional film formation process. Subsequently, the high-performance sensing properties of the porous $Co_3O_4$ NR arrays for ethanol gas and the gas-sensing mechanism will also be discussed.

## 2. Experimental

### 2.1. Synthesis

The process of preparing cobalt hydroxide was greatly simplified from our previous method [22]. All chemicals were of analytical grade and used as purchased without further purification. The typical experiments were as follow and the fabricating process is illustrated in Fig. 1(a): 4 mmol (1.16 g) of cobalt nitrate ($Co(NO_3)_2{\cdot}6H_2O$), 8 mmol (0.29 g) of ammonium fluoride ($NH_4F$) and 8 mmol (1.12 g) of hexamethylenetetramine ($C_6H_{12}N_4$, HMT) were dissolved in 40 ml high purity water (18.3 MΩ cm resistivity) under stirring at room temperature. After stirring for 10 min, the homogeneous solution was transferred into a 50 ml Teflon-lined stainless steel autoclave. Then, a piece of cleaned polycrystalline alumina ceramics plate (13 mm × 7 mm, 0.5 mm in thick) which have been plated Ag-Pd finger regions (five pairs, both the width and distance are 200 μm) as electrodes were immersed in the reaction solution against the inner wall of the autoclave and fixed by polyimide tapes. The autoclave was sealed and maintained at 95 °C for 24 h inside an electric oven. After cooling down to room temperature spontaneously, the substrate was removed, rinsed with distilled water several times in order to remove the free nanoparticle debris and the residual reactant, and dried at 60 °C under vacuum for 2 h. Finally, the as-prepared pink precursors were converted to $Co_3O_4$ via thermal decomposition after annealing at 450 °C in air for 4 h with a heating rate of 10 °C per minute. The obtained samples could be directly used for gas sensing measurements, and a top view of sensor substrate and the samples before and after annealing are shown in Fig. 1(b).

### 2.2. Characterization

The crystal phase identification were investigated by X-ray diffraction (XRD, Bede D1) system with Cu-$K_{\alpha1}$ radiation ($\lambda$ = 0.15406 nm) over the $2\theta$ range of 10–80°. The morphologies of both the precursor and calcined products were investigated using field emission scanning electron microscopy (FESEM, Hitachi S-4800) with an accelerating voltage of 5 kV. Further structural analysis of individual NR was carried out using high-resolution transmission electron microscopy (HRTEM, FEI F20) with an accelerating voltage of 200 kV. Fourier transform infrared spectroscopy (FTIR, TENSOR 27) was characterized with DTGS detector by making pellets with KBr powder. X-ray photoelectron spectroscopy (XPS, Thermo ESCALAB 250) measurement was performed with a monochromatic Al-Kα ($h\nu$ = 1486.6 eV) X-ray source. The electrical characteristics were measured at room temperature in the dark using a semiconductor parameter analyzer (Agilent E5270B) with the bias voltage range of −10 to 10 V.

### 2.3. Gas-sensing measurements

The gas-sensing properties of the $Co_3O_4$ sensors were performed on an intelligent gas sensing analysis system (CGS-1TP, Beijing Elite Tech Co., Ltd, China). The analysis system offered an external temperature control (from room temperature to 500 °C), which could conductively adjust the sensor temperature with a precision of 1 °C. The sensors were laid on the temperature control and pre-heated at different operating temperatures for about 30 min. Two probes were pressed on sensor electrodes by controlling the position adjustment in the analysis system. When the resistance of the sensor was stable, saturated target gas was injected into the

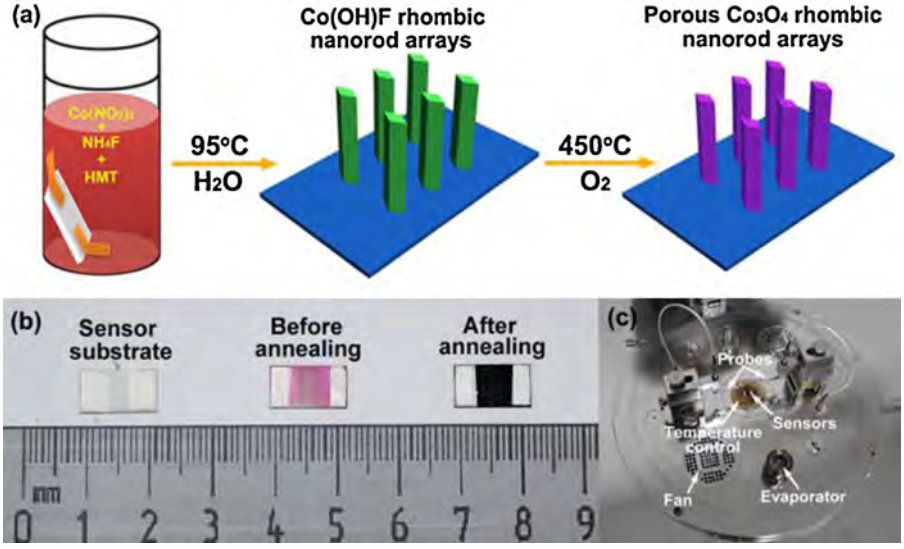


**Fig. 1.** (a) Schematic diagram of the fabricating process. (b) Top view of sensor substrate and sample sensors. (c) A photograph of the gas sensing analysis system.

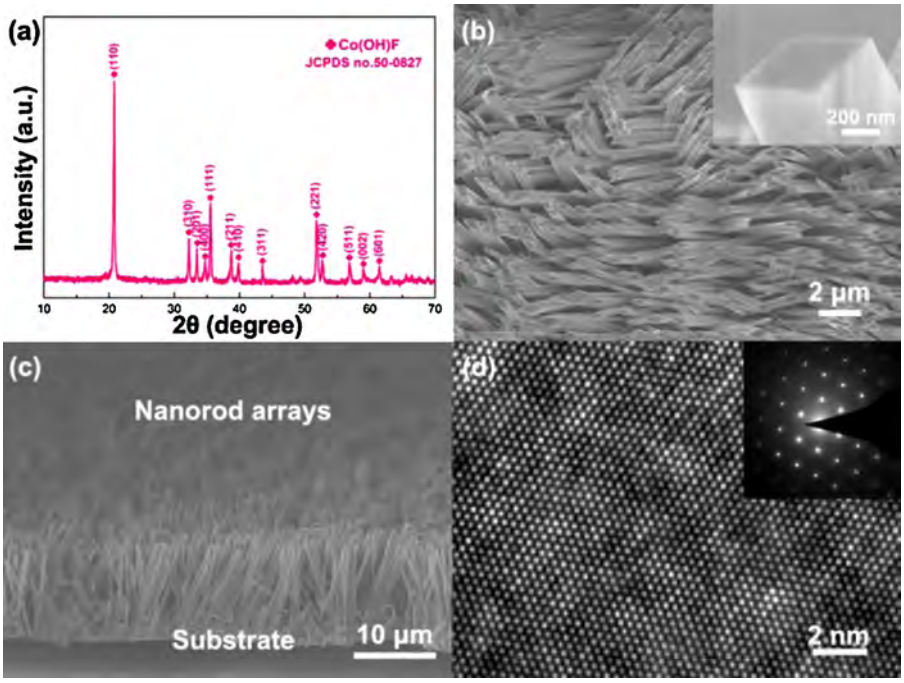


**Fig. 2.** Phase composition, morphological and structural characterization of the precursor: (a) XRD pattern of the as-prepared Co(OH)F; (b and c) SEM images of Co(OH)F NR arrays on the supporting substrate; and (d) HRTEM image of a Co(OH)F NR and the corresponding SAED pattern (inset).

test chamber (18 L in volume) by a micro-injector through a rubber plug. The saturated target gas was mixed with air (relative humidity was ~46%) by two fans. After the sensor resistance reached a new constant value, the test chamber was opened to recover the sensors in air. The sensor resistance and sensitivity were collected and analyzed by the system in real time. The photograph of the gas sensing analysis system is shown in Fig. 1(c). The gas response ($S$) was designated as the ratio $R_g/R_a$, where $R_g$ was a mixture of target gas and air and $R_a$ was the sensor resistance in air (base resistance). Response and recovery times were defined as the time needed for 90% of total resistance change on exposure to gas and air, respectively.

## 3. Results and discussion

### 3.1. Materials characterization

The phase composition, morphology and structure of the precursor obtained by the hydrothermal method were firstly investigated systematically. Fig. 2(a) shows the XRD pattern of the precursor, which is indexed as Co(OH)F. The pattern shows very sharp peaks, and all of the diffraction peaks are in good agreement with the standard Joint Committee on Powder Diffraction Standards (JCPDS) card No. 50-0827, which indicates that the precursor is a pure orthorhombic phase of Co(OH)F and has good crystallinity. From a typical SEM image of the precursor in Fig. 2(b), we can see that large-scale and high density arrays of Co(OH)F NRs are uniformly grown on the substrate. The inset of Fig. 2(b) shows that the NR arrays have a clear-cut rhombic contour with an average edge length of 400 nm and an induced edge angle of around 50°, and the surface of the NRs is smooth. The cross-sectional SEM image shown in Fig. 2(c) indicates that the Co(OH)F NR arrays with a length of about 15 μm are homogeneously well aligned. The HRTEM and corresponding SAED pattern in Fig. 2(d) and inset confirm the NRs to be single-crystalline.

To better understand the possible phase changes, the precursor was annealed at 450 °C for 4 h and analyzed by XRD and FTIR, respectively. The XRD patterns shown in Fig. 3(a) reveal that all

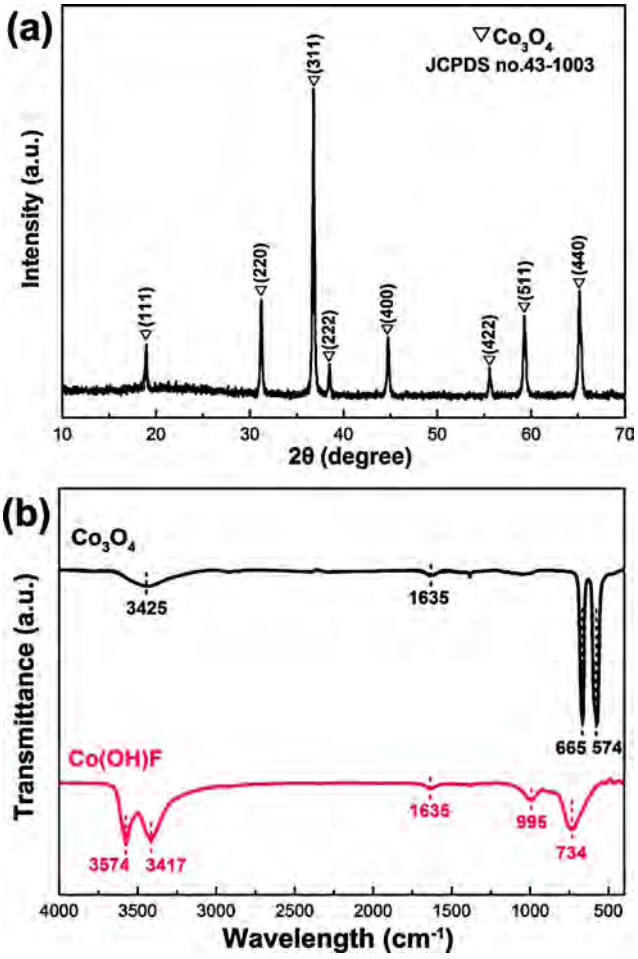


**Fig. 3.** (a) XRD patterns of the $Co_3O_4$ NR arrays. (b) FTIR spectra of the samples before and after annealing at 450 °C.

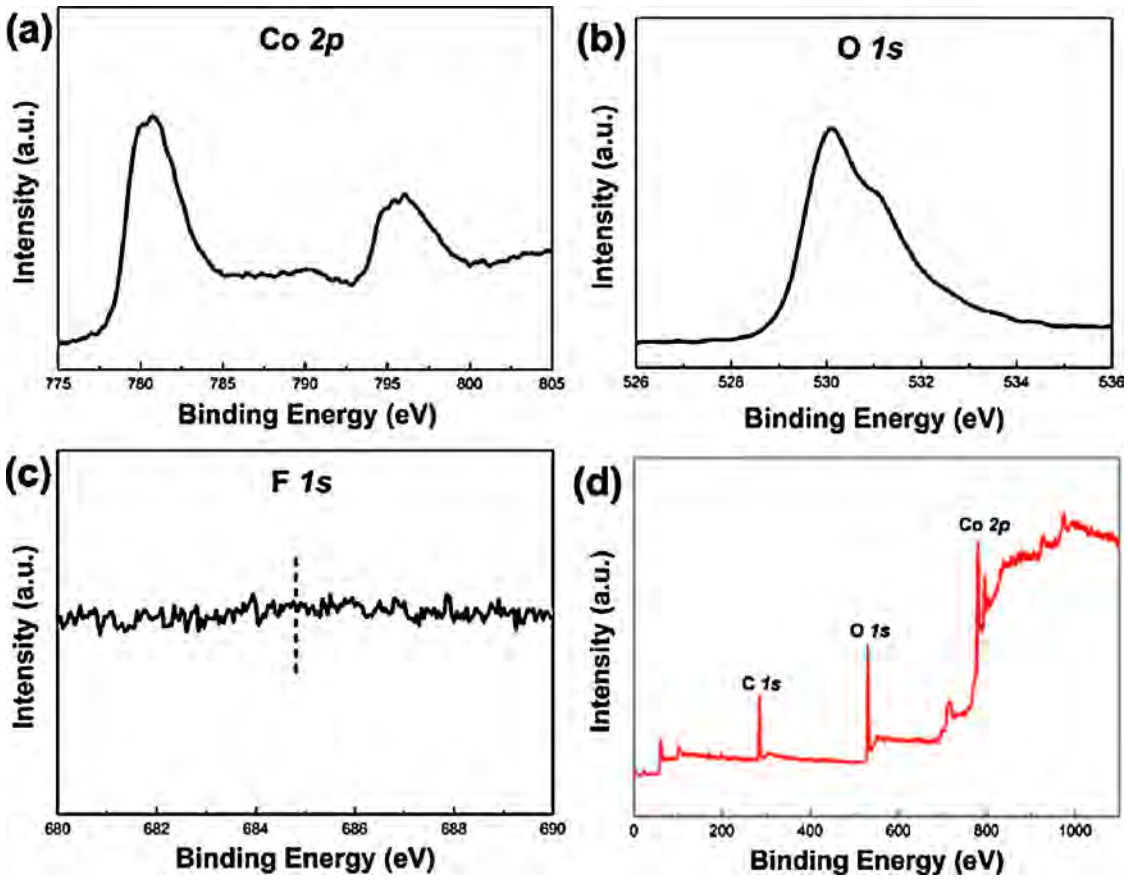


**Fig. 4.** XPS spectra of the $Co_3O_4$ NRs: slow scan spectra of (a) Co 2p, (b) O 1s and (c) F 1s; (d) full survey scan spectrum.

of the peaks correspond well to cubic spinel $Co_3O_4$ phase (JCPDS card No.43-1003) and no diffraction peaks of Co(OH)F are observed, which reveal the complete thermal conversion of the precursor Co(OH)F to $Co_3O_4$. Fig. 3(b) depicts the FTIR spectra of the samples before and after annealing, respectively. The strong peaks at 3574 $cm^{-1}$ and 1635 $cm^{-1}$ are attributed to the molecular water and hydrogen-bond O—H groups [11]. The shoulder vibration at 3417 $cm^{-1}$ can be assigned to the O—H groups interacting with fluoride. All the organic groups banding at 995 $cm^{-1}$ and 734 $cm^{-1}$ which belong to Co—OH and Co—F could be completely removed after calcination. Wide band at 3425 $cm^{-1}$ indicates the presence of water in the samples. Two new distinct peaks at 574 $cm^{-1}$ and 665 $cm^{-1}$ are related with the stretching vibrations of the metal oxygen bonds, which confirm the formation of the $Co_3O_4$ spinel oxide [11,23]. Thus, the FTIR spectroscopy results confirm the phase structure changes, which correspond with the XRD results.

The XPS measurement was carried out for further investigation of the chemical composition and the spectra is shown in Fig. 4. Fig. 4(a) shows the Co 2p spectra, and two peaks of each sample are similar, centered at 780.2 and 795.6 eV, corresponding to the Co $2p_{3/2}$ and Co $2p_{1/2}$. The gap between the peaks is about 15 eV (spin orbit splitting), which also corresponds to the standard $Co_3O_4$ spectra [24,25]. The major peak of O 1s observed in Fig. 4(b) is 530.1 eV, which can be attributed to the lattice oxygen of $Co_3O_4$. Besides, a small broadening peak centered at 532.0 eV corresponds to the absorbed species at the surface [24,26]. No F 1s peak at ~685 eV is found in Fig. 4(c), which can be assigned to the presence of Co(OH)F [4,22,27]. The full survey scan spectrum is shown in Fig. 4(d), and the result demonstrates that the sample is pure $Co_3O_4$.

Fig. 5 shows the SEM image of the as-prepared $Co_3O_4$ and a high-magnification image inset. The sample also maintained a basic shape of rhombic NRs, however, a coarse surface. Moreover, pores appeared on the surface, which may be formed due to the dehydration and lattice contraction occurring during the thermal treatment [28,29]. This change leads to the formation of the porous $Co_3O_4$ NRs through the thermal decomposition of the precursor. From these, it can be revealed that the synthesis includes two steps, the low temperature fluorine-mediated hydrothermal route of preparing rhombic Co(OH)F NR arrays and the pyrolysis of Co(OH)F precursor into porous $Co_3O_4$, without altering the original shape.

The crystallographic properties were examined and a typical TEM image in Fig. 6(a) indicates that a single NR has a diameter

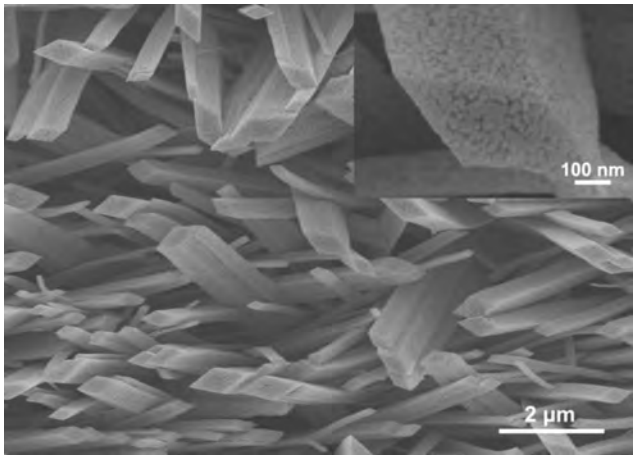


**Fig. 5.** SEM image of the rhombus-shaped $Co_3O_4$ NR arrays annealed at 450 °C (high-magnification inset).

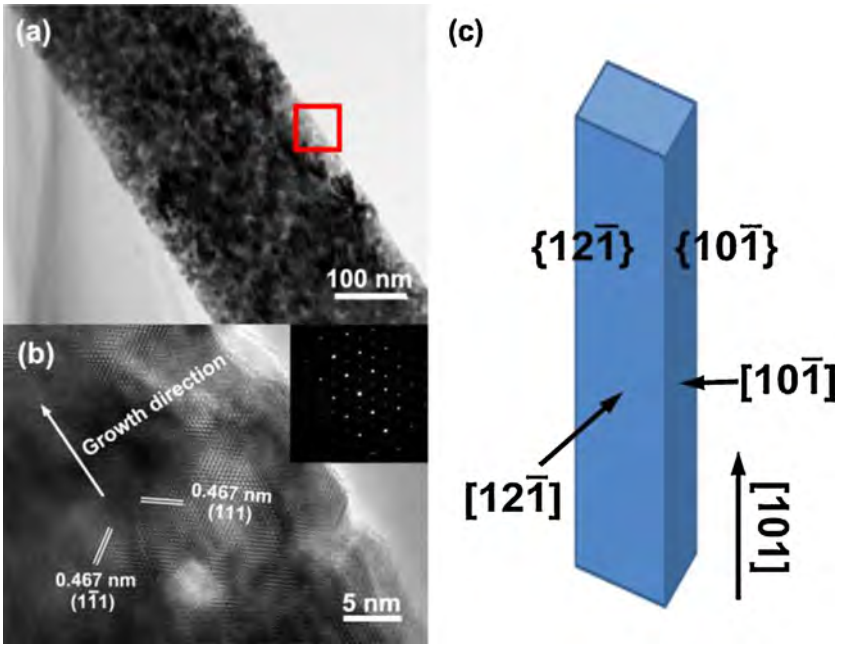


**Fig. 6.** (a) TEM image of a single rhombus-shaped $Co_3O_4$ NR annealed at 450 °C; (b) HRTEM image of the area indicated by the red rectangle in (a) and its SAED pattern (inset); (c) sketch map of the growth direction of a quasi-single-crystalline $Co_3O_4$ NR.

of ~400 nm and a porous structure with rough surfaces, which agrees with the SEM observations. The HRTEM image in Fig. 6(b) and the SAED pattern (inset in Fig. 6(b)) of the $Co_3O_4$ NR reveal that the $Co_3O_4$ NRs demonstrate highly oriented growth and quasi–single–crystalline nature. The set of (1–11) planes with a crossing lattice spacing of 0.467 nm with the included angle of 70.5 ° indicate that the directly exposed crystal plane open to us is {1,0,−1}. The SAED analysis further indicates that the NRs are with an axis perpendicular to the (1 1 1) plane, showing growth along the [1 0 1] direction. Combined with the results in our previous work [22], the structure of the $Co_3O_4$ NR is schematically drawn in Fig. 6(c). The rhombus-shaped $Co_3O_4$ NRs are enclosed by two equivalent {1,2,−1} crystal planes and two equivalent {1,0,−1} crystal planes.

### 3.2. Gas sensing properties

As a result of the large surface areas and porous structure revealed in the rhombus-shaped $Co_3O_4$ NR arrays, it is worthwhile to study its gas-sensing performance. The $Co_3O_4$ NR arrays directly grown on the Ag–Pd finger regions are randomly oriented, which provides electrical paths between the neighboring fingers. When these $Co_3O_4$ NRs are randomly oriented, the two electrodes are no longer electrically open. Furthermore, it is noteworthy that the as-prepared Co(OH)F NRs can still stick to the substrate firmly even after strong ultrasonication over 30 min, suggesting the robust adhesion between the NRs and the supporting substrate. After annealing, such contacts would be much stronger because of the improved crystallinity of the $Co_3O_4$ NRs. The intensive contact with the substrate would make it possible to use $Co_3O_4$ NRs directly as gas sensors without the conventional film formation process. Fig. 7 plots the current–voltage (*I*–*V*) characteristics between the two neighboring electrodes bridged by the $Co_3O_4$ NRs in the air. The current increased linearly with applied bias. Such linear behavior reveals good Ohmic contacts between the NRs and the electrodes, which is very important for the electrical properties of NRs because this ensures that all upcoming sensing behaviors of sensors represent the properties of the NRs but not the contact between the nanorods and the electrodes [10].

The optimal working temperature for maximum sensitivity was determined and the gas sensing performance is shown in Fig. 8. As the ethanol is injected, the resistivity of the sample increases exponentially, and recovers to their initial state after exposing them to air, in agreement with that of a typical *p*-type semiconductor in the entire working temperature range. The response was found to increase with the operating temperature, and then decrease with a further rise of the operating temperature. This behavior can be explained by the gas adsorption and desorption kinetics on the surface of $Co_3O_4$ or similar semiconducting metal oxides [30–32]. When the operating temperature is too low, the chemical activation of NRs is consequently small, leading to a very small response. When the operating temperature increases too much, some adsorbed gas molecules may escape before their reaction due to their enhanced activation, thus the response will decrease correspondingly. The gas sensor reaches the highest gas response at 160 °C, much lower than those reported for $Co_3O_4$ sensors [14–16].

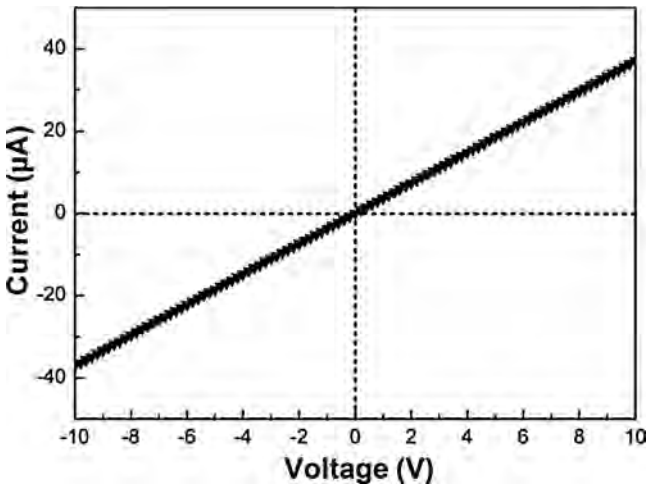


**Fig. 7.** *I*–*V* characteristics of the $Co_3O_4$ NR array-based gas sensor.

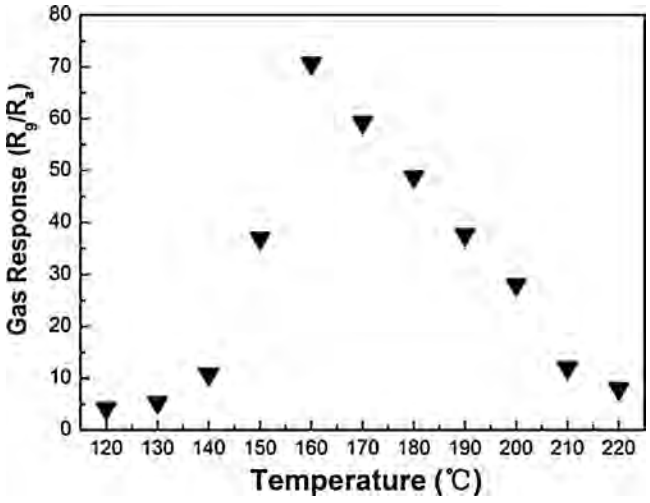


**Fig. 8.** Gas response of the $Co_3O_4$ sensor as a function of different working temperatures to 500 ppm ethanol.

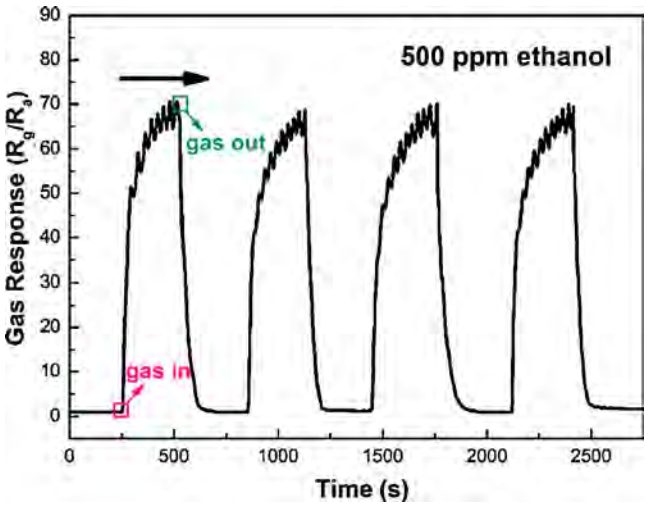


**Fig. 10.** The typical response and recovery curve of the $Co_3O_4$ sensor between 500 ppm ethanol and ambient air.

Fig. 9 shows the sensor response versus ethanol with concentrations ranging from 10 to 200 ppm at the optimal operating temperature of 160 °C. The response increases rapidly with increasing the concentration of ethanol. The result illustrates that the sensor could detect ethanol gas in a wide range of concentrations, starting with the minimum concentration of 10 ppm, which is below the limit imposed for a breath analyzer [15]. Moreover, the variation shows the nearly linear tendency, which confirms that the sensor is quantitatively for low concentration ethanol gas detection.

Fig. 10 shows typical response and recovery curves between 500 ppm ethanol and ambient air. The response undergoes a drastic ascent on the injection of ethanol vapor and is mostly recovered to its initial value after the test gas is released. Both response and recovery were very fast, taking about 90 and 60 s, respectively, which is effective in the rapid detection of ethanol. After several cycles of gas injection, full recovery to the initial response of the gas sensors remains the same, indicating good reproducibility of the as-synthesized NRs.

Fig. 11 shows the responses to several reducing gases at the operating temperature of 160 °C. The gas response to 500 ppm ethanol vapor is 70.7, which is significantly higher than all the other gases under the same concentration. The sensor shows a low response to methanol, acetone, xylene, benzene and toluene, and almost totally insensitive to CO, $H_2$, $CH_4$ and $NH_3$. The above results indicate that the selectivity of the sensor based on porous $Co_3O_4$ NR arrays is very high and the sensor shows high anti-interference ability. Despite the fact that the $Co_3O_4$ NR arrays-based sensor shows good response to ethanol, further investigation of the long-term stability of this gas device for real application as a sensor is still required.

The response of the sensor to 500 ppm ethanol is repeated for a period of 3 months with 30 times test as shown in Fig. 12. The mean response and standard error are calculated to be 71 and 10, showing a relative error of ~14%. Therefore, we can conclude that the stability of this material is good enough in long time detection of ethanol [21].

### 3.3. Gas sensing mechanism

The gas sensing mechanism for $Co_3O_4$ is widely ascribed to the change of electrical conductivity resulting from the chemical interaction of gas molecules with the surface which often involves gas adsorption, surface reaction, and desorption processes [10,16]. $Co_3O_4$ shows a highly conductive state in the air due to the holes, which are the main charge carriers for a *p*-type semiconductor. The

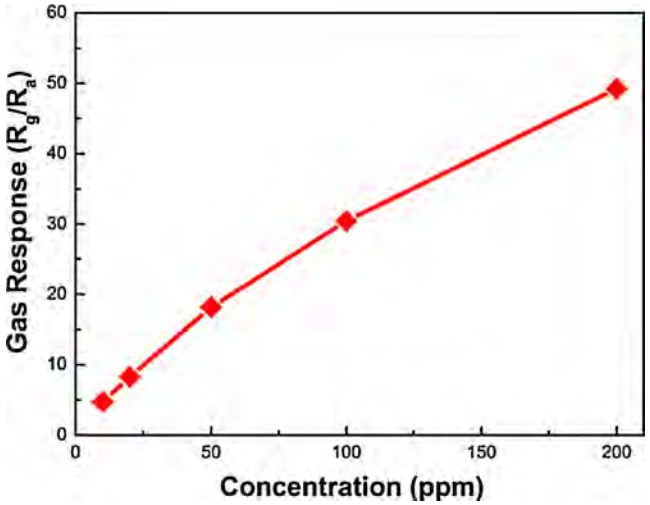


**Fig. 9.** Responses of the $Co_3O_4$ sensor to ethanol with concentrations ranging from 10 to 200 ppm at 160 °C.

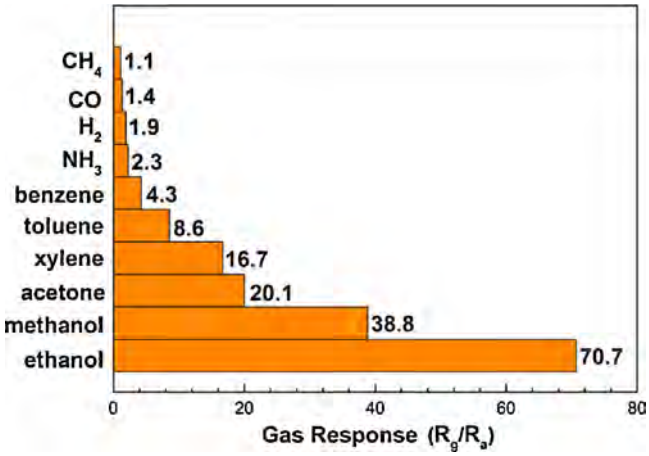


**Fig. 11.** The response curves of the $Co_3O_4$ sensor to several reducing gases with concentration of 500 ppm at 160 °C.

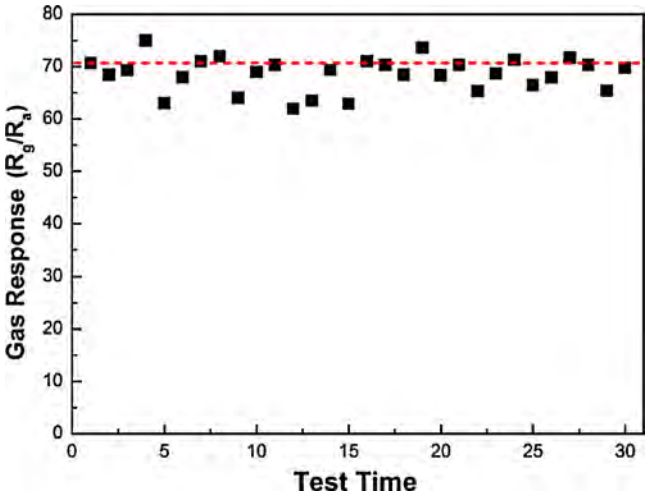


**Fig. 12.** The response of the $Co_3O_4$ sensor at 160 °C to 500 ppm ethanol (RH ~ 46%) repeated with 30 times test during three months.

surface of $Co_3O_4$ is readily covered with the monolayer configuration of negatively charged chemisorbed oxygen, even at low oxygen partial pressure or at temperatures up to 500 °C [33]. Thus, at the sensing temperature, the adsorption of negatively charged oxygen can generate the holes for conduction, which leads to the formation of a charge accumulation layer on the surface. Therefore, when the ethanol is introduced into the test chamber, the charge carrier accumulation layer near the surface is thinned by the electrochemical interaction between $O^-$ and gas molecules, which releases free electrons and neutralizes the holes in the $Co_3O_4$, and increases the resistances of the $Co_3O_4$ NRs until a dynamic equilibrium condition is obtained [16]. Hereafter, when the ethanol flow stopped, oxygen molecules in the air are adsorbed on the surface of the $Co_3O_4$ NRs, and sensor resistance decreased to their initial values.

In our case, we believe that the high-performance for ethanol detection can be attributed to the unique structure of $Co_3O_4$ NR arrays with a variety of favorable features. First, the direct growth of $Co_3O_4$ NRs on supporting substrates can facilitate every NR to participate in the gas sensing reaction [14,22]. Second, the tunable pore size allow the gas molecules to easily penetrate and adsorb on the surface of the nanorods, leading to fast response and recovery as well as high sensitivity [10,34]. Third, the high crystallinity of the $Co_3O_4$ NRs dramatically increases the long-term stability of the sensors [10]. Fourth, the high surface-to-volume ratio of NR arrays can provide more active reaction sites for adsorption and transportation of gas molecules [35,36]. Fifth, the open space of the NR arrays between individual NRs allows for easy contact and diffusion of the gas molecular into the inner region of the NRs [20,37].

## 4. Conclusions

We have successfully synthesized rhombus-shaped $Co_3O_4$ NR arrays via a facile fluorine-mediated hydrothermal route involving the formation of Co(OH)F as precursor and the thermal conversion to porous $Co_3O_4$. The NR arrays could be directly served as gas sensors without the conventional film formation process owing to good Ohmic contacts with the electrodes and intensive contact with the substrate. The NR array-based gas sensor showed high-performance to ethanol detection. The response to 500 ppm ethanol reached ~71 and the optimal working temperature was as low as 160 °C. Moreover, the sensor could detect ethanol in a wide range of concentrations starting with a low detection limit, which exhibited good reproducibility and stability. The high-performance owes to the one-dimension structure, nano-porosity, large specific surface area, unique rhombic morphology, good crystallinity and the open space of nanorod arrays. The results demonstrate that the rhombus-shaped $Co_3O_4$ NR arrays are very promising for the fabrication of cost effective and high-performance gas sensors for ethanol.

## Acknowledgements

This work was supported by National Natural Science Foundation of China 51072181, Science and Technology Department of Zhejiang Province Project No. 2010R50020.

## References

[1] X. Xie, Y. Li, Z.Q. Liu, M. Haruta, W. Shen, Low-temperature oxidation of CO catalysed by $Co_3O_4$ nanorods, Nature 458 (2009) 746–749.
[2] S.K. Meher, G.R. Rao, Ultralayered $Co_3O_4$ for high-performance supercapacitor applications, Journal of Physical Chemistry C 115 (2011) 15646–15654.
[3] D. Barreca, M.C. Yusta, A. Gasparotto, C. Maccato, J. Morales, A. Pozza, et al., Cobalt oxide nanomaterials by vapor-phase synthesis for fast and reversible lithium storage, Journal of Physical Chemistry C 114 (2010) 10054–10060.
[4] D. Barreca, D. Bekermann, E. Comini, A. Devi, R.A. Fischer, A. Gasparotto, et al., Plasma enhanced-CVD of undoped and fluorine-doped $Co_3O_4$ nanosystems for novel gas sensors, Sensors and Actuators B 160 (2011) 79–86.
[5] W.Y. Li, L.N. Xu, J. Chen, $Co_3O_4$ nanomaterials in lithium-ion batteries and gas sensors, Advanced Functional Materials 15 (2005) 851–857.
[6] D. Barreca, P. Fornasiero, A. Gasparotto, V. Gombac, C. Maccato, A. Pozza, et al., CVD $Co_3O_4$ nanopyramids: a nano-platform for photo-assisted $H_2$ production, Chemical Vapor Deposition 16 (2010) 296–300.
[7] D. Bekermann, A. Gasparotto, D. Barreca, C. Maccato, M. Rossi, R. Matassa, et al., Epitaxial-like growth of $Co_3O_4$/ZnO Quasi-1D nanocomposites, Crystal Growth and Designs 12 (2012) 5118–5124.
[8] D. Barreca, A. Gasparotto, O.I. Lebedev, C. Maccato, A. Pozza, E. Tondello, et al., Controlled vapor-phase synthesis of cobalt oxide nanomaterials with tuned composition and spatial organization, CrystEngcomm 12 (2010) 2185–2197.
[9] D. Barreca, E. Comini, A. Gasparotto, C. Maccato, A. Pozza, C. Sada, et al., Vapor phase synthesis, characterization and gas sensing performances of $Co_3O_4$ and Au/$Co_3O_4$ nanosystems, Journal of Nanoscience and Nanotechnology 10 (2010) 8054–8061.
[10] H. Nguyen, S.A. El-Safty, Meso- and Macroporous $Co_3O_4$ nanorods for effective VOC gas sensors, Journal of Physical Chemistry C 115 (2011) 8466–8474.
[11] Y. Liu, G. Zhu, B. Ge, H. Zhou, A. Yuan, X. Shen, Concave $Co_3O_4$ octahedral mesocrystal: polymer-mediated synthesis and sensing properties, CrystEngcomm 14 (2012) 6264–6270.
[12] J. Park, X. Shen, G. Wang, Solvothermal synthesis and gas-sensing performance of $Co_3O_4$ hollow nanospheres, Sensors and Actuators B 136 (2009) 494–498.
[13] H.N. Hieu, N.M. Vuong, H. Jung, D.M. Jang, D. Kim, H. Kim, et al., Optimization of a zinc oxide urchin-like structure for high-performance gas sensing, Journal of Materials Chemistry 22 (2012) 1127–1134.
[14] K.I. Choi, H.R. Kim, K.M. Kim, D. Liu, G. Cao, J.H. Lee, $C_2H_5OH$ sensing characteristics of various $Co_3O_4$ nanostructures prepared by solvothermal reaction, Sensors and Actuators B 146 (2010) 183–189.
[15] A.M. Cao, J.S. Hu, H.P. Liang, W.G. Song, L.J. Wan, X.L. He, et al., Hierarchically structured cobalt oxide ($Co_3O_4$): the morphology control and its potential in sensors, Journal of Physical Chemistry B 110 (2006) 15858–15863.
[16] J.W. Yoon, J.K. Choi, J.H. Lee, Design of a highly sensitive and selective $C_2H_5OH$ sensor using p-type $Co_3O_4$ nanofibers, Sensors and Actuators B 161 (2012) 570–577.
[17] C. Sun, S. Rajasekhara, Y. Chen, J.B. Goodenough, Facile synthesis of monodisperse porous $Co_3O_4$ microspheres with superior ethanol sensing properties, Chemical Communications 47 (2011) 12852–12854.
[18] S. Hwang, H. Kwon, S. Chhajed, J.W. Byon, J.M. Baik, J. Im, et al., A near single crystalline $TiO_2$ nanohelix array: enhanced gas sensing performance and its application as a monolithically integrated electronic nose, Analyst 138 (2012) 443–450.
[19] T.J. Hsueh, Y.W. Chen, S.J. Chang, S.F. Wang, C.L. Hsu, Y.R. Lin, et al., ZnO nanowire-based CO sensors prepared on patterned ZnO:Ga/$SiO_2$/Si templates, Sensors and Actuators B 125 (2007) 498–503.
[20] J.X. Wang, X.W. Sun, Y. Yang, H. Huang, Y.C. Lee, O.K. Tan, et al., Hydrothermally grown oriented ZnO nanorod arrays for gas sensing applications, Nanotechnology 17 (2006) 4995–4998.
[21] A.K. Srivastava, Detection of volatile organic compounds (VOCs) using $SnO_2$ gas-sensor array and artificial neural network, Sensors and Actuators B 96 (2003) 24–37.
[22] W.M. Mei, J. Huang, L.P. Zhu, Z.Z. Ye, Y. Mai, J.P. Tu, Synthesis of porous rhombus-shaped $Co_3O_4$ nanorod arrays grown directly on a nickel substrate with high electrochemical performance, Journal of Materials Chemistry 22 (2012) 9315–9321.
[23] X.H. Xia, J.P. Tu, Y.Q. Zhang, Y.J. Mai, X.L. Wang, C.D. Gu, et al., Freestanding $Co_3O_4$ nanowire array for high performance supercapacitors, RSC Advances 2 (2012) 1835–1841.
[24] C.V. Schenck, J.G. Dillard, J.W. Murray, Surface analysis and the adsorption of Co(II) on goethite, Journal of Colloid Interface Science 95 (1983) 398–409.

[25] N. Yan, L. Hu, Y. Li, Y. Wang, H. Zhong, X. Hu, et al., $Co_3O_4$ nanocages for high-performance anode material in lithium-ion batteries, Journal of Physical Chemistry C 116 (2012) 7227–7235.
[26] C.C. Li, X.M. Yin, T.H. Wang, H.C. Zeng, Morphogenesis of highly uniform $CoCO_3$ submicrometer crystals and their conversion to mesoporous $Co_3O_4$ for gas-sensing applications, Chemistry of Materials 21 (2009) 4984–4992.
[27] A. Gasparotto, D. Barreca, D. Bekermann, A. Devi, R.A. Fischer, P. Fornasiero, et al., F-Doped $Co_3O_4$ photocatalysts for sustainable $H_2$ generation from water/ethanol, Journal of the American Chemical Society 133 (2011) 19362–19365.
[28] X.W. Lou, D. Deng, J.Y. Lee, L.A. Archer, Thermal formation of mesoporous single-crystal $Co_3O_4$ nano-needles and their lithium storage properties, Journal of Material Chemistry 18 (2008) 4397–4401.
[29] H. Yu, D. Wang, M.Y. Han, Top-Down Solid-Phase Fabrication of Nanoporous Cadmium Oxide Architectures, Journal of the American Chemical Society 129 (2007) 2333–2337.
[30] L. Liu, S. Li, J. Zhuang, L. Wang, J. Zhang, H. Li, et al., Improved selective acetone sensing properties of Co-doped ZnO nanofibers by electrospinning, Sensors and Actuators B 155 (2011) 782–788.
[31] M. Ghasdi, H. Alamdari, CO sensitive nanocrystalline $LaCoO_3$ perovskite sensor prepared by high energy ball milling, Sensors and Actuators B 148 (2010) 478–485.
[32] J. Herrán, O. Fernández-González, I. Castro-Hurtado, T. Romero, G. Mandayo, E. Castaño, Photoactivated solid-state gas sensor for carbon dioxide detection at room temperature, Sensors and Actuators B 149 (2010) 368–372.
[33] S. Pokhrel, C.E. Simion, V. Quemener, N. Bârsan, U. Weimar, Investigations of conduction mechanism in $Cr_2O_3$ gas sensing thick films by ac impedance spectroscopy and work function changes measurements, Sensors and Actuators B 133 (2008) 78–83.
[34] T. Wagner, S. Haffer, C. Weinberger, D. Klaus, M. Tiemann, Mesoporous materials as gas sensors, Chemical Society Reviews 42 (2013) 4036–4053.
[35] Y. Cui, Q. Wei, H. Park, C.M. Lieber, Nanowire nanosensors for highly sensitive and selective detection of biological and chemical species, Science 293 (2001) 1289–1292.
[36] X.Y. Xue, S. Yuan, L.L. Xing, Z.H. Chen, B. He, Y.J. Chen, Porous $Co_3O_4$ nanoneedle arrays growing directly on copper foils and their ultrafast charging/discharging as lithium-ion battery anodes, Chemical Communications 47 (2011) 4718–4720.
[37] Y. Li, B. Tan, Y. Wu, Mesoporous $Co_3O_4$ nanowire arrays for lithium ion batteries with high capacity and rate capability, Nano Letters 8 (2007) 265–270.

## Biographies

**Zhen Wen** received his BS degree at China University of Mining and Technology in 2011. He is currently pursuing PhD degree at Zhejiang University. His research interests are in the area of nano-materials and their application in gas sensors.

**Liping Zhu** received her BSc (1988) and MSc (1991) degrees in Materials Science from Zhejiang University. She studied in Hiroshima University in Japan as a doctoral student from 1998 to 2002. Then she joined the Materials Department of Zhejiang University since 2002. Her current research interests include semiconductor materials, photo-electronic thin films, nano-materials and their application in devices.

**Weimin Mei** received BS degree at Wuhan University of Technology in 2010. He is currently pursuing MS degree at Zhejiang University. His research interests are in the area of nano-materials and their application in lithium ion batteries.

**Liang Hu** received BS degree at China University of Geosciences in 2009. He is currently pursuing PhD degree at Zhejiang University. His current fields of interests include doping mechanism and defect ferromagnetism behavior of ZnO colloidal nanocrystal.

**Yaguang Li** received BS degree at Yanshan University in 2010. He is currently pursuing MS degree at Zhejiang University. His research interests are in the area of nano-materials and their application in catalysis.

**Luwei Sun** received PhD degree at Zhejiang University in 2011. He is presently a postdoctor at Zhejiang University. His research interests are in the field of ZnO-based nanomaterials.

**Hui Cai** received BS degree at Yanshan University in 2011. He is currently pursuing MS degree at Zhejiang University. His current fields of interests include design and synthesis of semiconductor thin films.

**Zhizhen Ye** received his BS degree in Electrical Engineering, received his MS degree and his Ph.D. in Optical Engineering from Zhejiang University in 1981, 1984 and 1987 respectively. He has been a professor of materials science and engineering since 1994. His research interests are in the area of heterogrowth and devices fabrication of silicon-based thin films.